Amino Acids
DOI 10.1007/s00726-014-1695-1

ORIGINAL ARTICLE

L-cysteine-induced fabrication of spherical titania nanoparticles within poly(ether-imide) matrix

Hojjat Seyedjamali · Azadeh Pirisedigh

Received: 20 November 2013 / Accepted: 8 February 2014

Abstract In the presented study, a new L-cysteine-containing diamine is synthesized and fully characterized and its application for the in situ sol–gel fabrication of poly (ether-imide)/titania nano hybrid materials is investigated. The electron microscopic photographs (TEM, FE-SEM and AFM) of the resulted materials confirm the production of spherical nanoparticles with well dispersion and narrow particle size distribution which is a usual challenge in the sol–gel methods. In addition to the positive effects on the particles morphology, the existence of amino acid containing pendant groups in the structure of polymer chains led to the comprehensive interaction with titania phase. As a result, the improvement in the flexibility of polymer backbone (as one of the most serious difficulties in polyimides processing) is obtained while its thermal stability dose is not sacrificed (confirmed by TGA and DSC techniques).

Keywords L-cysteine · Poly(ether-imide) · Titania · Sol–gel · Morphology

Introduction

The insertion of naturally occurring species into the chemical structure of artificial materials is a powerful strategy to increase their biodegradability, bioactivity and/or biocompatibility (Liang et al. 2011; Bao et al. 2013; Wu et al. 2007; Singh and Lilard 2009; Xue et al. 2011; Park et al. 2013a). With the rapidly growing applications of polymer/inorganic nano hybrid materials in various areas from aerospace industry to tissue engineering, their biotic modification seems to be promising (Kango et al. 2013; Park et al. 2013b; Okamoto and John 2013). Among the artificial materials, polyimides (PIs) and PI matrix nanocomposites possess the specific situations due to their excellent thermal, chemical, mechanical, optical and dielectric properties (Liaw et al. 2013; Xiao et al. 2009; Jang et al. 2007). The combination of excellent physicochemical properties of PIs and multi-functionalistic nature of titania (TiO_2) provides one of the most important classes of modern materials with versatile applications, especially when titania is nanosized, low aggregated, well-graded and spherical in shape (Lee et al. 2009; Tsai et al. 2008; Missan et al. 2010; Rajesh et al. 2013). The homogenization of intrinsically dissimilar polymer-inorganic couples, which affects intensively the particles morphology, is attainable via either the chemical modification of inorganic nanoparticles (e.g., the use of silane linkages) or utilization of the polymers suitable to construct the physical interactions in organic–inorganic interfaces, namely, the site isolation concept (Yoshida et al. 1997).

The in situ sol–gel technique is a powerful and of course straightforward method for the fabrication of nanoparticles within the polymer grounds by means of site isolation concept; however, it typically suffers from the production of non-spherical particles with limited size gradation due to the low organic–inorganic compatibility (Cao et al. 2013; Pandini et al. 2013; Morselli et al. 2012). On the other hand, the insertion of traditional bulky pendant groups in the structure of PIs—to overcome their general low processability—may worsen the organic–inorganic compatibility and disrupt the

H. Seyedjamali (✉)
Department of Environmental Engineering, University of Environment, 31746-74761 Karaj, Islamic Republic of Iran
e-mail: seyedjamali@yahoo.com

A. Pirisedigh
Department of Chemistry and Petrochemical Engineering, Standard Research Institute, 31745-139 Karaj, Islamic Republic of Iran

Published online: 01 March 2014

consistency in the morphology of inorganic nanoparticles as they increase the hydrophobicity of PI matrixes (Song et al. 2013; Vanherck et al. 2013; Seyedjamali and Pirisedigh 2012a).

Recently, we have reported the in situ synthesis of titania nanoparticles within a polymer matrix including L-leucine as a fraction of polyimide main chains (Seyedjamali and Pirisedigh 2011a). In a separate work, we examined the incorporation of amino acids in the chemical structure of pendant groups which gave improved results in terms of better dispersion and created nanoparticles with more spherical shapes attributed to the more flexibility of pendant groups (Seyedjamali and Pirisedigh 2011b). Since the later investigation had been carried out using L-phenylalanine, we did a third study on the use of L-leucine as a fraction of pendant groups and the experiments proved the superior results not only due to the more elasticity of pendant groups regiochemistry but also to the additional flexibility of L-leucine in comparison with L-phenylalanine (Seyedjamali and Pirisedigh 2012b). L-cysteine as the only naturally occurring amino acid containing—SH functional group has the ability to bind more effectively to the variety of metals and metal oxides (Su et al. 2010; Lv et al. 2012). The binding nature could be a combination of thiolate formation, (-S-metal), H bond or simple dipole–dipole interactions (Muir and Idriss 2013; Ataman et al. 2011; Lachheb et al. 2012). In addition, the secondary interaction of thiol group with the surface plays an important role on the interaction strength (Muir and Idriss 2013; Ataman et al. 2011). Thus, as the extension of our investigations, we decided to use L-cysteine fractions in the pendant group of PI matrix. Herein, we wish to report the full synthesis and characterization of a new L-cysteine containing diamine monomer and its application for the in situ sol–gel fabrication of new poly(ether-imide)/titania nano hybrid materials with superior particles morphology in terms of their shapes, dispersion and grading. Although the existence of naturally occurring amino acids in the structure of polymers may increase their biological activities (Katsarava 2003; Aït-Haddou et al. 2004; Sanda and Endo 1999), the investigations of this potential biological are not the subject of current report.

Materials and methods

Materials

All chemicals were purchased from Fluka Chemical Co. (Buchs, Switzerland), Aldrich Chemical Co. (Milwaukee, WI), Riedel–deHaen AG (Seelze, Germany) and Merck Chemical Co. 4,4′-oxydiphthalic anhydride (ODPA) was recrystallized from acetic anhydride and then dried in a vacuum oven at 125 °C overnight. *N,N*-dimethylformamide (DMF) was dried over barium oxide, followed by fractional distillation. Tetraethyl orthotitanate ($Ti(OEt)_4$) and acetylacetone (acac) were employed as received.

Instruments

Proton nuclear magnetic resonance (^{1}H-NMR, 500 MHz and ^{13}C-NMR, 125 MHz) spectra were recorded in DMSO-d_6 solution using a Bruker (Germany) Avance 500 instrument. FT-IR spectra were recorded on 400D IR spectrophotometer (Japan). The spectra were obtained using KBr pellets. The vibrational transition frequencies are reported in wave numbers (cm^{-1}). Band intensities are assigned as weak (w), medium (m) and strong (s). Thermal gravimetric analysis (TGA) data were taken on Perkin Elmer in nitrogen atmosphere at a heating rate of 20 °C min^{-1}. Differential scanning calorimetry (DSC) data were recorded on a DSC-PL-1200 instrument at a heating rate of 20 °C min^{-1} in nitrogen atmosphere. The glass transition temperatures (T_g)s were read at the middle of the transition in the heat capacity taken from the heating DSC traces. The X-ray diffraction (XRD) patterns were recorded by employing a Philips X'PERT MPD diffractometer (Cu Kα radiation: $\lambda = 0.154056$ nm at 40 kV and 30 mA) over the 2θ range of 20–80° at a scan rate of 0.05° min^{-1}. Transmission electron microscopy (TEM) images were recorded using a JEOL JEM-2000 operating at 200 kV. Field emission scanning electron microscopy (FE-SEM) was acquired by JEOL JSM-6700S Japan operating at an accelerating voltage of 1.5 or 5.0 kV. The sample was prepared by drop casting an acetone suspension onto mica substrate and then coated with gold. Atomic force microscopy (AFM) topographic images were obtained using Digital Multimode Instruments Nanoscope III (Digital Instrument Inc., USA) with noncontact tapping mode with a silica probe (NSC 11) and a frequency of 463 kHz. UV–visible absorbance spectra were obtained from Perkin UV–VIS lambda 850 spectrometer.

Synthesis of aromatic diamine monomer

*Methyl 2-(3,5-dinitrobenzamido)-3-mercaptopropanoate (**3**) synthesis*

Although, a production pathway has been reported previously for compound **3** (Metais et al. 1997), our synthesis was based on the procedure described as follows: to a chloroform (50 mL) solution of 3.0 g (17.5 mmol) 3,5-dinitrobenzoyl chloride (**2**), 4.03 g (17.5 mmol) of L-cysteine methyl ester hydrochloride (**1**) and 4 mL of Et_3N were added and stirred at room temperature until the complete conversion monitored by TLC (50:50

ethylacetate:*n*-hexane). Then, the mixture was washed with distilled water for three times. After that the organic phase was separated and dried over calcium chloride, the dinitro compound (**3**) was precipitated by rotary evaporation of chloroform and recrystallized from ethylacetate/n-hexane (5.24 g, 91 %). ^{1}H-NMR, ^{13}C-NMR and the other characterization details have been reported previously (Metais et al. 1997).

*N-(3-mercapto-1-oxo-1-(phenylamino)propan-2-yl)-3,5-dinitrobenzamide (**4**) synthesis*

A 50-mL round-bottomed flask equipped with a reflux condenser was charged with 5 g of compound dinitro **3** (15.2 mmol), 1.5 mL of freshly distilled aniline (1.53 g; 16 mmol) and 10 mL of DMF and refluxed overnight. Then, DMF was removed under reduced pressure and the precipitate was washed with 0.5 M aqueous solution of HCl (50:1 v/v) to precipitate **4** as a yellow powder which was washed with distilled water and vacuum dried (5.3 g, 90 %) mp 152–153 °C,$[\alpha]_D^{25} = +64.7$ (0.05 g in 10 mL of DMF); FT-IR (KBr): 3,343 (m), 3,100 (m), 3,070 (m), 2,967 (m), 2,620 (m), 2,555 (m), 2,498 (m), 1,692 (s), 1,673 (s), 1,601 (s), 1,503 (s), 1,447 (m), 1,280 (s), 1,255 (s), 1,069 (m), 1,035 (m), 1,020 (m), 919 (w), 865 (w), 801 (m), 718 (s), 691 (m) cm^{-1}. ^{1}H-NMR (500 MHz, DMSO, d_6): δ 1.47 (s, 1H, SH), 3.27 (d, 1H, CH, $J = 6.33$ Hz), 3.50 (d, 1H, CH, $J = 6.07$ Hz), 4.91 (dd, $J_1 = 7.55$, $J_2 = 6.21$, 1H, CH), 9.04 (s, 1H, Ar–H), 9.13 (s, 2H, Ar–H), 7.63–7.71 (m, 5H, Ar–H), 8.97 (s, 1H, amide NH), 9.50 (s, 1H, amide N–H) ppm. ^{13}C-NMR (125 MHz, DMSO, d_6): δ 35.44 (CH_2), 54.93 (CH), 102.15 (Ar), 103.23 (Ar), 122.15 (Ar), 129.44 (Ar), 129.91 (Ar), 135.19 (Ar), 136.48 (Ar), 151.74 (Ar), 167.22 (C=O), 172.37 (C=O) ppm. Elemental analysis calculated for $C_{16}H_{14}N_4O_6S$ (390.37 g mol^{-1}): C, 49.23 %; H, 3.61 %; N, 14.35 %. Found: C, 49.05 %; H, 3.85 %; N, 14.17 %.

*3,5-Diamino-N-(3-mercapto-1-oxo-1-(phenylamino)propan-2-yl)benzamide (**5**) synthesis*

In a 50-mL two necked round-bottomed flask equipped with a reflux condenser and a dropping funnel, 5 g of dinitro compound **4** (12.8 mmol), 0.5 g of Pd–C 10 % and 20 mL of DMF were added and heated slowly until 50 °C. Then, 25 mL of ethanol solution of hydrazine monohydrate 80 % (1:1 v/v) was added slowly (over 60 min) via the dropping funnel and the mixture was stirred vigorously. After the complete addition of hydrazine monohydrate, the mixture was refluxed for 1 h and filtered while hot. Diamine **5** was obtained by removal of DMF under reduced pressure. The products were recrystallized from absolute ethanol and vacuum dried (3.9 g, 93 %). mp 184–187 °C (dec.), $[\alpha]_D^{25} = +23.1$ (0.05 g in 10 mL of DMF). FT-IR (KBr): 3,441 (m), 3,363 (m), 3,295 (s), 3,212 (s), 3,160 (s), 3,101 (s), 3,072 (m), 2,967 (m), 2,618 (m), 2,557 (m), 2,503 (m), 1,690 (s), 1,671 (s), 1,604 (s), 1,505 (s), 1,445 (m), 1,281 (s), 1,253 (s), 1,072 (m), 1,036 (m), 1,019 (m), 921 (w), 869 (w), 802 (m), 721 (s), 694 (m), 653 (m) cm^{-1}. ^{1}H-NMR (500 MHz, DMSO, d_6): δ 1.46 (s, 1H, SH), 3.29 (d, 1H, CH, $J = 6.47$ Hz), 3.52 (d, 1H, CH, $J = 5.94$ Hz), 4.93 (dd, $J_1 = 7.63$, $J_2 = 6.15$, 1H, CH), 5.51 (s, 4 H, NH_2), 6.05 (s, 1H, Ar–H), 6.62 (s, 2H, Ar–H), 7.59–7.67 (m, 5H, Ar–H), 8.81 (s, 1H, amide NH), 9.49 (s, 1H, amide N–H) ppm. ^{13}C NMR (125 MHz, DMSO-d_6), δ (ppm): δ 35.72 (CH_2), 54.55 (CH), 102.11 (Ar), 103.64 (Ar), 122.13 (Ar), 129.45 (Ar), 130.07 (Ar), 135.12 (Ar), 136.19 (Ar), 149.65 (Ar), 167.73 (C=O), 172.38 (C=O) ppm. Elemental analysis calculated for $C_{16}H_{18}N_4O_2S$ (330.40 g mol^{-1}): C, 58.16 %, H, 5.49 %, N, 16.96 %. Found: C, 57.94 %; H, 5.68 %; N, 16.62 %.

Fabrication of NCs

A 25-mL round-bottomed flask was charged with 3.5 g of diamine **5** (10.6 mmol) and 22 mL of DMF was added to dissolve the diamine compound completely. The solution was cooled to 0 °C and 3.29 g of ODPA (10.6 mmol) was added in several portions and stirred for 1 h at 0 °C and 2 h at room temperature under N_2 atmosphere, to yield the poly(amic acid) (PAA) solution. ($Ti(OEt)_4$) was dissolved in acac with a molar ratio of 1:4 prior to use. Then, according to the wanted titania percentages (3–15 wt%), the required amounts of $Ti(OEt)_4$/acac were added, assuming the complete conversion to TiO_2 particles. The homogenization was carried out with vigorous stirring for 15 h. Then, thin films of mixed PAA containing various titanate precursors were cast onto the glass plates. Obtained films were annealed in an electric oven at 50, 75, 100, 125, 150, 175, 200, 225, and 250 °C for 30 min each and 300 °C for 10 h and then were cooled very slowly and removed from glass surfaces. Abbreviations as PEI/T0, PEI/T3, PEI/T5, PEI/T10 and PEI/T15 corresponded to the pure polymer matrix and nanocomposites containing 3–15 wt% titania contents, respectively.

Results and discussion

Monomer synthesis and characterization

L-cysteine-containing diamine monomer (**5**) was synthesized according to the sequence shown in Scheme 1. Methyl ester derivative of L-cysteine was used due to the limited organosolubility of its corresponding carboxylic

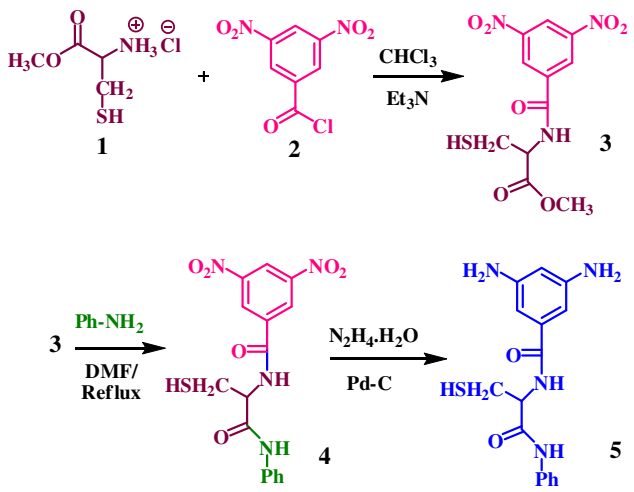

Scheme 1 Synthesis of L-cysteine containing diamine monomer (**5**)

acid compound. In the next step, ester functional group was converted to amide using overnight refluxing with aniline. This transformation leads to the more capability of diamine to construct H bond lattice via amide protic sites.

In FT-IR spectrum of diamine **5** (Fig. 1), the strong absorption peaks appeared at 1,690 and 1,671 cm^{-1} are related to the stretching of two carbonyl double bonds related to the amide functional groups. The absorption peaks related to the amine and amide NH bonds are observable at 3,200–3,450 cm^{-1}. Full assignments of ^{1}H-NMR and ^{13}C-NMR spectrums are presented in Figs. 2 and 3, respectively, which show full agreement with the chemical structure of diamine **5**.

Nanocomposites fabrication

Diamine **5** was reacted with ODPA in dry DMF at room temperature for the fabrication of the corresponding poly(amic acid) (PAA) which subsequently was mixed with different quantities of tetraethyl orthotitanate/acac to form the homogeneous solutions as the sol (Scheme 2). The role of acac is to prevent the fast conversion to the gel which leads to the fabrication of nanoparticles with more consistency. After the film production via evaporation of the solvent from glossy surfaces, the crude materials were annealed up to 300 °C. During the thermal treatment, the amic acid fractions were converted to the imide functions and generated water—as the condensation byproduct—turned the titanate precursor into the titania particles. The deliberate bit by bit heating and cooling of materials through the fabrication process let the titania particles to form the more spherical shapes. It was verified that the fast thermal operation has the reverse consequences on the geometric order of the created particles. Furthermore, the existence of several functions in the chemical structure of polymer matrix with the ability to interact with inorganic phase has definite results on the particles morphology.

According to the high tendency of species including thiol functions for metal catalyzed disulfide bond formation especially in the presence of humidity and/or oxygen (Mezyk 1995; Leong et al. 2013), the materials were kept away from both external moisture and air. However, solubility tests showed the small decrease in the solubility of fabricated materials with the increase in titania contents attributable to the creation of partials disulfide cross links between polymer chains and/or two pendant groups of a particular chain (Fig. 4). Possible mechanism (Fujii et al. 1987) for the intermolecular and intramolecular metal-mediated disulfide bonds formation is presented in scheme 3.

Spectroscopic study of nano hybrid materials

The confirmation of thermal cyclization of amic acid moieties to imide functions is demonstrable via either FT-IR spectra or TGA experiments. In the FT-IR spectrums of PAA (Fig. 5), the broad absorption peak at

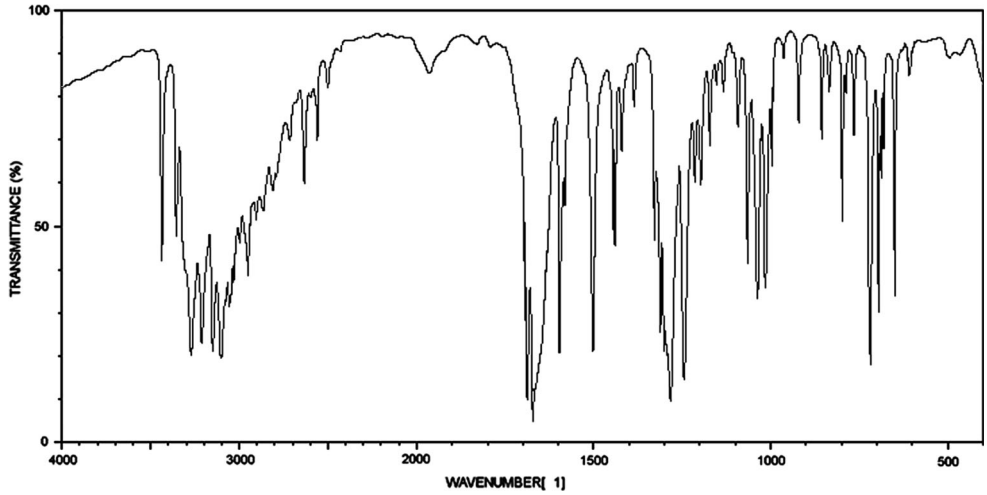

Fig. 1 FT-IR spectrum of diamine monomer **5**

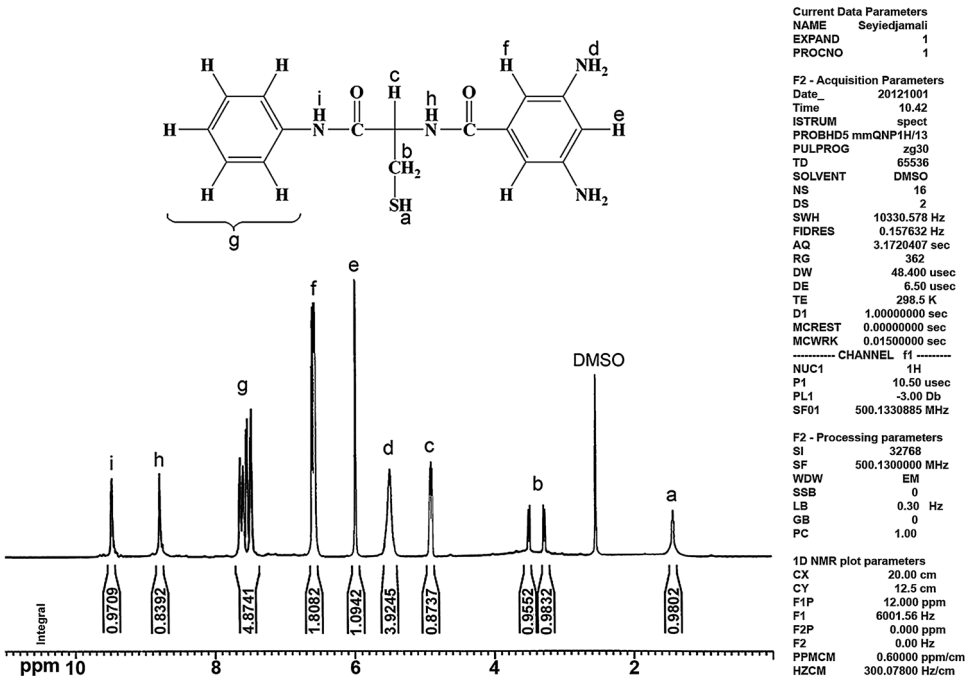

Fig. 2 ^{1}H-NMR spectrum of diamine monomer **5**

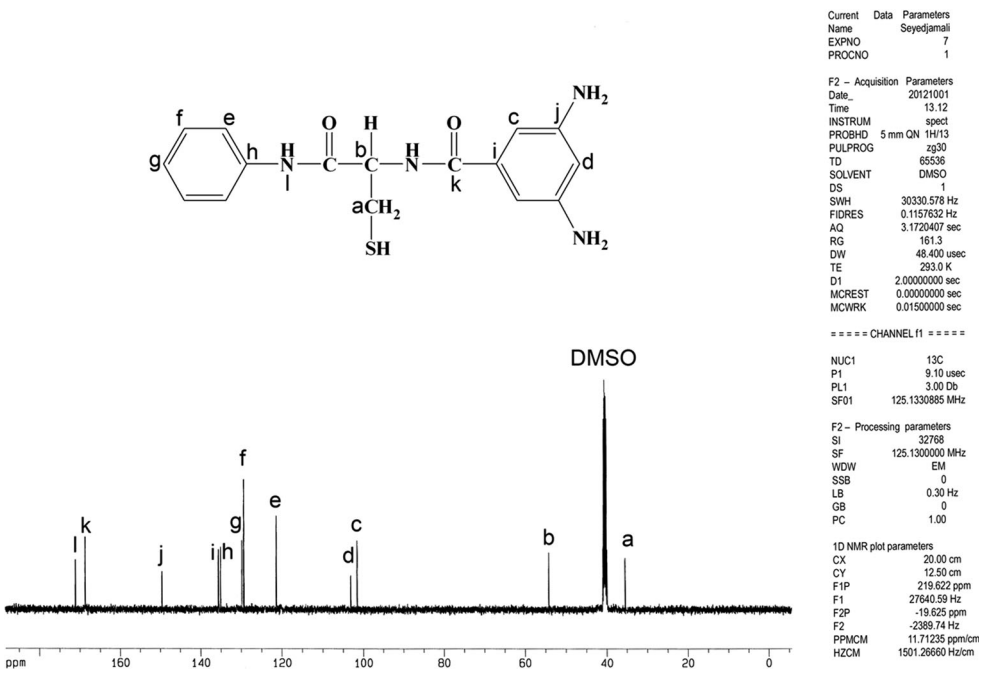

Fig. 3 ^{13}C-NMR spectrum of diamine monomer **5**

2,350–2,550 cm^{-1} refers to the carboxylic acid functions which disappeared after thermal operation (PEI/T0 or PEI/T10) confirming the complete imidization. The absorption peaks related to the stretching of imide ring are assigned in Fig. 5. The FT-IR spectrum of PEI/T10 is illustrated representatively which shows a strong absorption peak related to the titania phase (Ti–O stretching). The other noticeable absorption peaks are the stretching of thiol S–H bond which appear at 2,598 cm^{-1} for PEI/T0 indicating the free S–H bond and at 2,489 cm^{-1} for PEI/T10 attributable to the S–H bond involved in the interaction with TiO_2 phase. The FT-IR spectra of the other fabricated hybrid materials were more or less the same.

The UV–Vis spectroscopy of fabricated nanocomposites was carried out as well. Accordingly, the more titania contents have led to the fewer UV transmission percent (Fig. 6). The more absorption efficiency could be discussed by both more aggregation of titania particles and formation

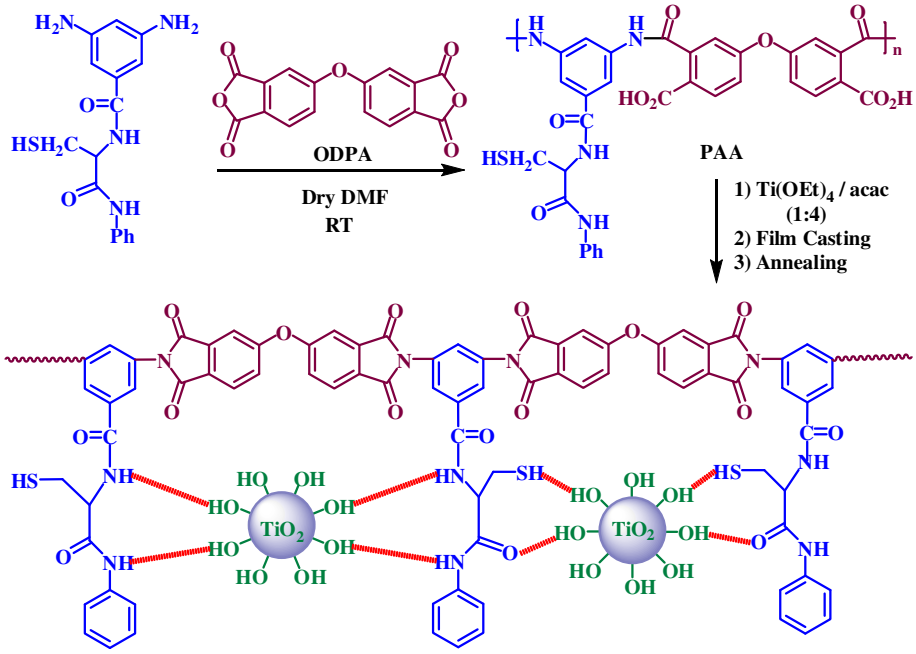

Scheme 2 Fabrication sequences for nano hybrid materials with different titania contents

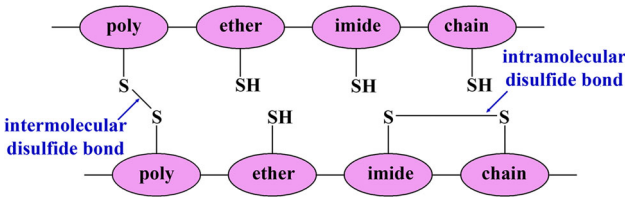

Fig. 4 Hypothetical schema representing of disulfide cross-link formation

of titanium ion–acac complex (Liaw and Chen 2007; Que et al. 2000). However, the complex mechanism may be negligible, subsequent to the gelation step. Although the color of resulted materials was ranged from yellow (in PEI/T3) to brown (in PEI/T15), all the materials were completely transparent. While they block out the lights with higher frequency, like a sun glass, the visible region of light spectrum is transparent. This behavior could be useful for the applications where the polymer/titania nano hybrid materials are used for absorption of UV irradiations, e. g. photoelectrochemical applications, photocatalysts, optical filters and antireflective coatings (Li et al. 2002, 2013; Chang et al. 2009; Tsai et al. 2008, 2006; Liaw and Chen 2007; Chiang and Whang 2003; Chen et al. 2014; Ehsani et al. 2014; Li and Ni 2013; Muthirulan et al. 2013; Gupta et al. 2013).

Morphological study

Various apparatus were applied to investigate the size, sized distribution, shape and grading of nanoparticles created within the polymer matrix through the sol–gel process. Although the sol–gel technique provides a straightforward method for producing of nanoparticles, it suffers the weak control of their morphology. Thus, the introduction of new strategies for modification of this method is promising. The TEM photographs of nanocomposites with various titania concentrations are provided in Fig. 7. As it may be seen, the well-dispersed and spherical nanoparticles are created specially in the lower titania contents.

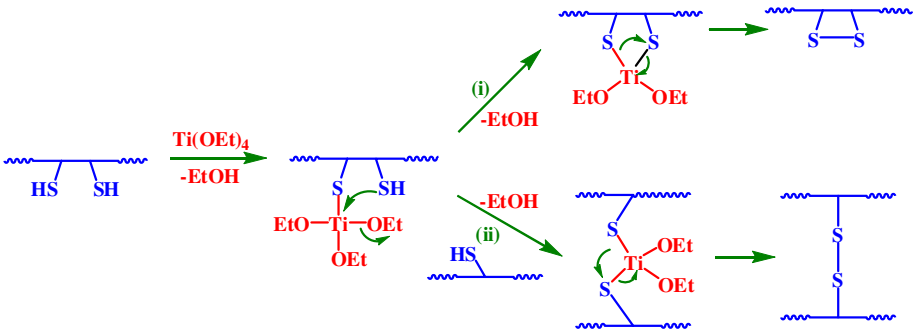

Scheme 3 Proposed mechanism for (*i*) intramolecular and (*ii*) intermolecular disulfide bonds formation

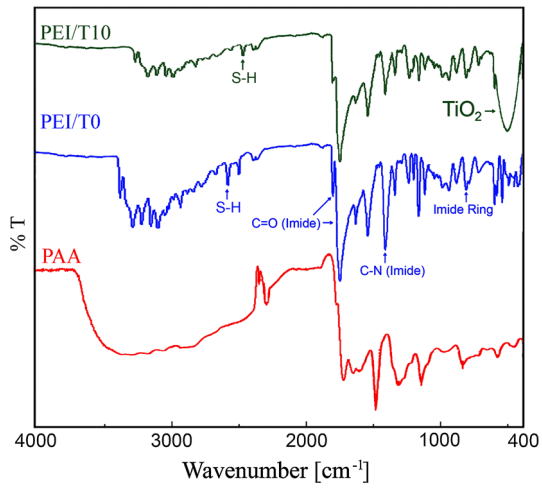

Fig. 5 FT-IR spectra of PAA, PEI/T0 and PEI/T10 as the examples

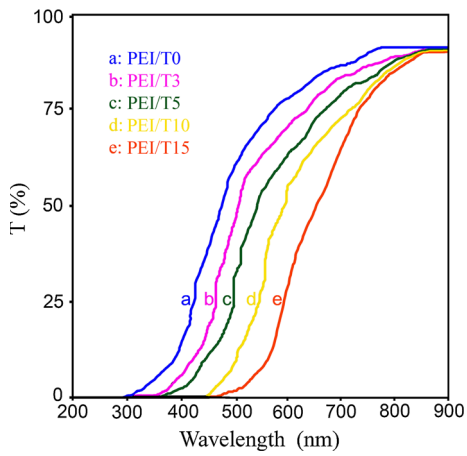

Fig. 6 UV–vis spectra of PEI/T0-PEI/T15

According to the sized distribution diagrams (Fig. 8), the fine particles grading is obtained which may be attributed to the comprehensive organic–inorganic interactions and the control of the reaction rate in the gelation step by means of both the slow thermal imidization and the use of acac as the chelating agent. The use of L-cysteine containing diamine monomer including several protic (amide NH and SH fractions) and dipolar (carbonyl groups) functionalities has led to form a three-dimensional network of organic–inorganic interactions. The site isolation concept (Yoshida et al. 1997) in a widespread state is responsible for the more geometrical ordering and well dispersion as well as the narrow particle size distributions. In comparison with the similar investigations, the presented PI could be considered as a beneficial matrix for the in situ sol–gel fabrication of TiO_2 nanoparticles in terms of the superior distribution, more consistency and spherical particles morphology (Tsai et al. 2008, 2006; Liaw and Chen 2007; Chiang and Whang 2003; Seyedjamali and Pirisedigh 2011a, b; Seyedjamali and Pirisedigh 2012a, b).

Figure 9 illustrates the FE-SEM photograph of PEI/T5 as a representative issue as well as graphical illustration of organic/inorganic interaction and the severe tendency of poly(ether-imide) back bone to wrap the titania nanoparticles. In addition to the H bonds or dipole–dipole interactions, the use of ODPA as a dianhydride monomer including a flexible ether function and the existence of bulky pendant groups including aliphatic fractions in the structure of monomer may be the other facilitators for surrounding titania particles more efficiently.

The investigation of surface topography was done using AFM imaging technique too. The observable convexities in the AFM image of PEI/T3 (Fig. 10) which are attributed to the titania nanoparticles reveal that (a) nanoparticles are created not only in the ventricle of nanocomposite but also in its surface, and (b) surface nanoparticles are well-dispersed and relatively spherical in shape.

The XRD analysis was performed to verify the crystallinity of nano hybrid materials. The typical XRD patterns for pure anatase titania PEI/T0 and PEI/T10 are presented in Fig. 11. The peaks appeared at $2\theta = 16.0°$, 19.2° and 19.9° are related to the diffractions of partial crystalline poly(ether-imide) matrix. The absence of these peaks in the spectra of hybrid materials (e.g., PEI/T10) could be attributed to the tough organic–inorganic interaction which suppresses the fractional crystallinity of polymer matrix and flatten the bulging section of XRD patterns.

Thermal properties

The thermal analyses of fabricated nano hybrid materials were done using TGA and DSC experiments which are presented in Fig. 12 and Table 1, respectively. Accordingly, the fabricated nanocomposites with higher titania contents showed elevated thermal resistances by means of T_5, T_{10}, T_g and char yields.

A large descend in the thermogram of PAA is apparent which is attributed to the generation of H_2O molecules along with the thermal imidization. This thermogram returns to the flat pattern at 300 °C confirming the complete imidization. This observation is in agreement with the FT-IR data where the strong broad carboxylic acid peak in the spectrum of PAA was omitted in PEI/T0 which proves the complete imidization spectroscopically. This temperament was observed in FT-IR spectra of the other entries (only PEI/T10 is shown) as a result of the comprehensive thermal imidization of amic acid moieties. A comparison between the TGA thermograms (Fig. 12) of PEI/T0 and PEI/T3-PEI/T15 shows that there is a relatively large gap between the thermal stabilities of pure polymer matrix (b) and the other nano hybrid materials (c–f) whereas the

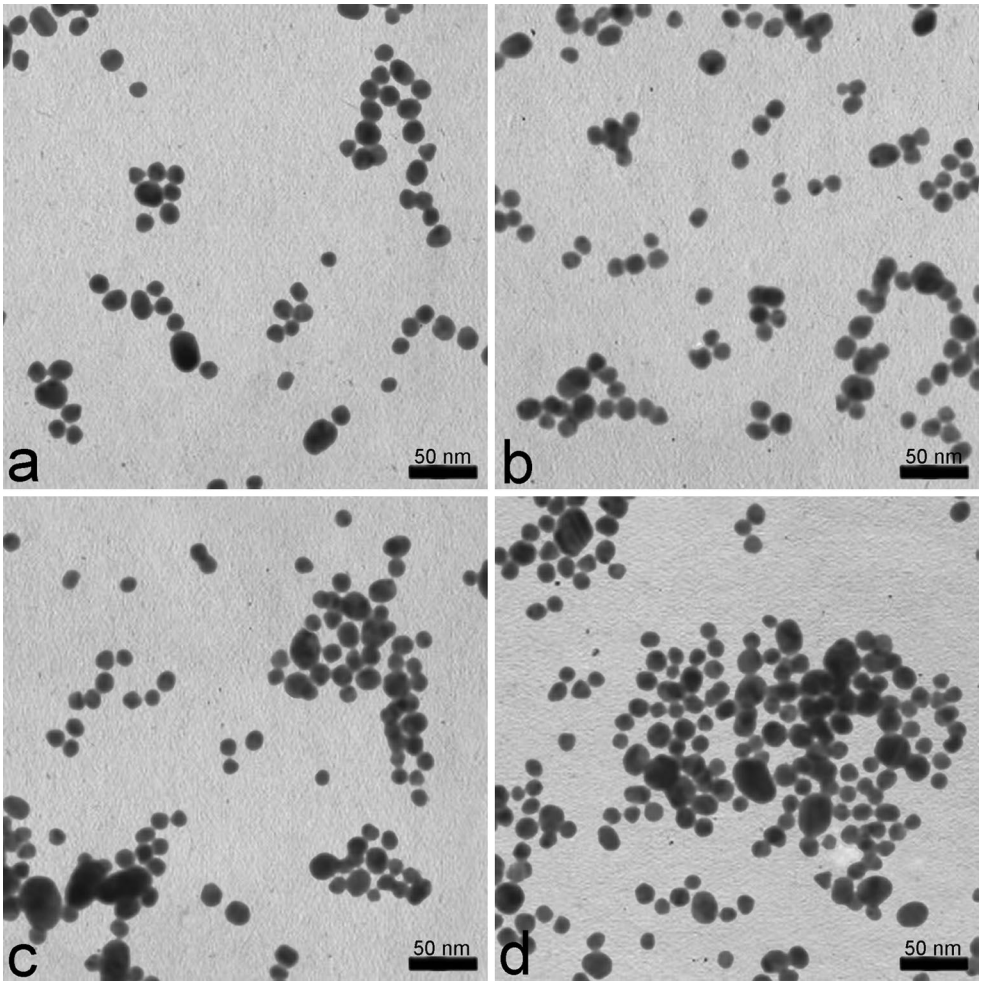

Fig. 7 TEM photographs of nanocomposites with 3 % (**a**), 5 % (**b**), 10 % (**c**) and 15 % (**d**) titania contents

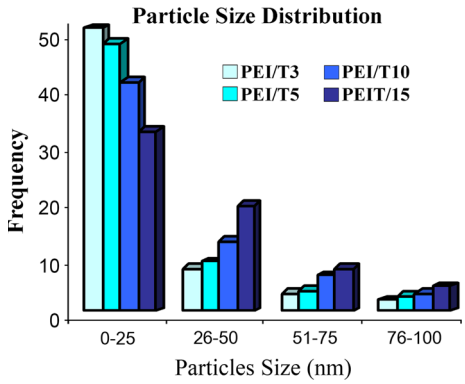

Fig. 8 Particle size distribution diagrams for fabricated nano hybrid materials

difference between the nano hybrid materials (c–f) is slighter. This observation reveals that the origin of the thermal stability is the construction of organic/inorganic interactions and not merely the existence of inorganic phase as an intrinsically more heat resistant fraction, otherwise a linear relationship between the concentration of titania and thermal stability should be observed. Furthermore, the T_g amount (193 °C) for pure PI matrix shows that it enjoys more processability while the comparison of its T_5, T_{10} and CY with those in PEI/T3 confirms the positive and intensive effects of inorganic phase on the compensation of thermal stability. The growth of T_g values with the increase in titania concentration could be discussed by more limited segmental movements caused by the strong L-cysteine-titania interaction in the materials with more titania contents.

Conclusions

A new L-cysteine containing diamine monomer is synthesized and fully characterized via spectroscopic and elemental analysis techniques. The application of the stated diamine for the in situ sol–gel fabrication of a new series of

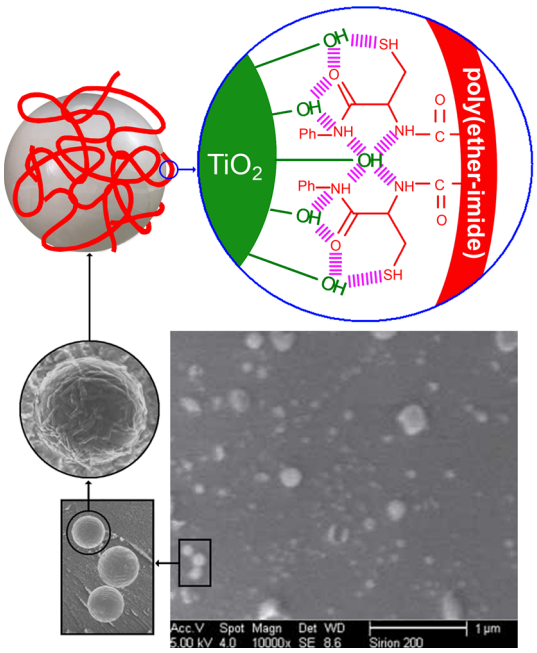

Fig. 9 Typical FE-SEM image of PEI/T15

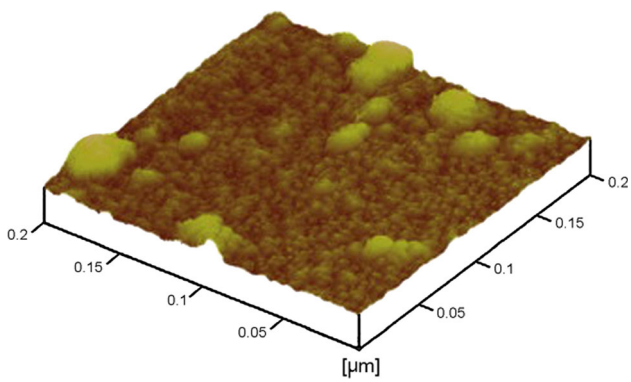

Fig. 10 Exemplar AFM topographic image of PEI/T15

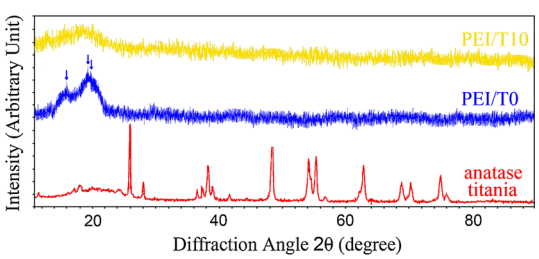

Fig. 11 XRD patterns of anatase titania, pure polymer matrix and a typical nanocomposite

PI/titania nanocomposites with the improved morphological features is reported. In comparison with the similar works the perfection in grading, dispersion and the globular shape of nanoparticles in a sol–gel manner is achieved while the thermal stability of PIs was not sacrificed. The significance of this achievement refers to:

(a) An improvement in processability as a sever challenge associated with the PIs applications is done without the increase in the organic nature of polymer.
(b) L-cysteine-induced improvement in the control of nanoparticles morphology as the most serious problem of the sol–gel manners offers a powerful, simple and inexpensive way for the in situ fabrication of nanocomposite materials.
(c) With the high and increasing consumptions of PI/titania nano hybrid materials in various modern areas, the presentation of their superior varieties is promising.
(d) The usual destructive effects of pendant groups on the thermal stability of PIs are compensated via the construction of strong interaction with inorganic phase which has an exciting coincident as the more spherical and well-distributed nanoparticles.

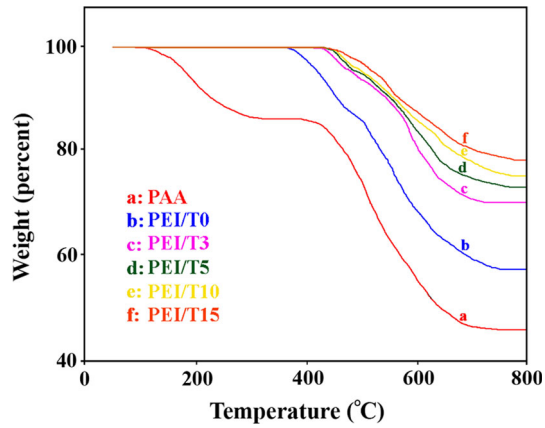

Fig. 12 TGA thermograms of PAA, pure polymer matrix and PEI/T3-PEI/T15

Table 1 Thermal analysis of nanocomposites

Material	T_5^a (°C)	T_{10}^b (°C)	T_g (°C)	CY^c (%)
PEI/T0	417	422	193	46
PEI/T3	468	538	244	69
PEI/T5	473	544	249	73
PEI/T10	476	548	257	75
PEI/T15	478	551	262	79

TGA; at heating rate of 10 °C min^{-1} and DSC; at heating rate of 20 °C min^{-1} in nitrogen atmosphere

[a] Decomposition temperature for 5 % weight loss

[b] Decomposition temperature for 10 % weight loss

[c] Char Yields, weight percentage of material left undecomposed at 800 °C

(e) Due to the existence of L-cysteine moieties in the structure of PI matrixes, they expected to show biological activities which could be the subject of further investigations.

Acknowledgments Financial support for this work from Research Affairs Division University of Environment; Standard Research Institute and Iran nanotechnology Initiative Council and National Elite Foundation (NEF) is greatly acknowledged.

Conflict of interest The authors declare that they have no competing financial interests.

References

Aït-Haddou H, Leeder SM, Gagne MR (2004) Amino-acid containing metallomonomers copolymerized into porous organic polymers: applicability to allylic alkylation catalysis. Inorg Chim Acta 357:3854–3864

Ataman E, Isvoranu C, Knudsen J, Schulte K, Andersen JN, Schnadt J (2011) Adsorption of L-cysteine on rutile TiO_2(110). Surf Sci 605:179–186

Bao Y, Shen G, Liu H, Li Y (2013) Fabrication of gold nanoparticles through autoreduction of chloroaurate ions by thermo- and pH-responsive amino acid-based star-shaped copolymers. Polymer 54:652–660

Cao J, Zhu Q, Dou J, Li C, Chen W, Li Z (2013) Controlling sol-gel polymerization to create bowl-shaped polysilsesquioxane particles with a kippah structure. Polymer 54:2493–2497

Chang WL, Su HW, Chen WC (2009) Synthesis and properties of photosensitive polyimide–nanocrystalline titania optical thin films. Eur Polym J 45:2749–2759

Chen CL, Chan TW, Su SC, Teng H, Lee YL (2014) High performance solid-state dye-sensitized solar cells based on poly(acrylonitrile-co-vinyl acetate)/TiO_2 nanoparticles redox electrolytes. J Power Sources 247:406–411

Chiang PC, Whang WT (2003) The synthesis and morphology characteristic study of BAO-ODPA polyimide/TiO_2 nano hybrid films. Polymer 44:2249–2254

Ehsani A, Adeli S, Babaei F, Mostaanzadeh H, Nasrollahzadeh M (2014) Electrochemical and optical properties of TiO_2 nanoparticles/poly tyramine composite film. J Electroanal Chem 713:91–97

Fujii N, Otaka A, Funakoshi S, Bessho K, Watanabe T, Akaji K, Yajima H (1987) Studies on Peptides. CLI. Syntheses of cystine-peptides by oxidation of S-protected cysteine-pPeptides with thallium(III) trifluoroacetate. Chem Pharm Bull 35:2339–2347

Gupta KK, Mishra PK, Srivastava P, Gangwar M, Nath G, Maiti P (2013) Hydrothermal in situ preparation of TiO_2 particles onto poly(lactic acid) electrospun nanofibres. Appl Surf Sci 264:375–382

Jang W, Shin D, Choi S, Park S, Han H (2007) Preparation, morphology and properties of acylchloride-grafted multiwall carbon nanotubes/fluorinated polyimide composites. Polymer 48:2130–2143

Kango S, Kalia S, Celli A, Njuguna J, Habibi Y, Kumar R (2013) Surface modification of inorganic nanoparticles for development of organic–inorganic nanocomposites. Prog Polym Sci 38:1232–1261

Katsarava R (2003) Active polycondensation: from peptide chemistry to amino acid based biodegradable Polymers. Macromol Symp 199:419–429

Lachheb H, Dappozze F, Houas A, Guillard C (2012) Adsorption and photocatalytic degradation of cysteine in presence of TiO_2. J Photochem Photobiol A Chem 246:1–7

Lee C, Kim I, Shin H, Kim S, Cho J (2009) Nonvolatile resistive switching memory properties of thermally annealed titania precursor/polyelectrolyte multilayers. Langmuir 25:11276–11281

Leong JX, Daud WRW, Ghasemi M, Liew KB, Ismail M (2013) Ion exchange membranes as separators in microbial fuel cells for bioenergy conversion: a comprehensive review. Renew Sustain Energy Rev 28:575–587

Li F, Ni X (2013) Improving poly(3-hexylthiophene)-TiO_2 heterojunction solar cells by connecting polypyrrole to the TiO_2 nanorods. Sol Energy Mater Sol Cell 118:109–115

Li L, Qinghua L, Jie Y, Xuefeng Q, Wenkai W, Zikang Z, Zongguang W (2002) Photosensitive polyimide (PSPI) materials containing inorganic nano particles (I)PSPI/TiO_2 hybrid materials by sol–gel process. Mater Chem Phys 74:210–213

Li Z, Gan M, Qiu W, Fu D, Li S, Bai Y (2013) Synthesis and anticorrosion performance of poly(2,3-dimethylaniline)–TiO_2 Composite. Prog Org Coat 76:1161–1167

Liang JZ, Tang CY, Zhou L, He L, Tsui CP (2011) Melt density and flow property of PDLLA/nano-$CaCO_3$ bio-composites. Compos B 42:1897–1900

Liaw CW, Chen KP (2007) Preparation and characterization of poly(imide siloxane) (PIS)/titania(TiO_2) hybrid nanocomposites by sol–gel processes. Eur Polym J 43:2265–2278

Liaw DJ, Wang KL, Huang YC, Lee KR, Lai JY, Ha CS (2013) Advanced polyimide materials: syntheses, physical properties and applications. Prog Polym Sci 37:907–974

Lv K, Hu J, Li X, Li M (2012) Cysteine modified anatase TiO_2 hollow microspheres with enhanced visible-light-driven photocatalytic activity. J Mol Catal A Chem 356:78–84

Metais E, Overman LE, Rodriguez MI, Stearns BA (1997) Halide-terminated *N*-acyliminium ion-alkyne cyclizations: a new construction of carbacephem antibiotics. J Org Chem 62:9210–9216

Mezyk SP (1995) Direct rate constant measurement of radical disulphide anion formation for cysteine and cysteamine in aqueous solution. Chem Phys Lett 235:89–93

Missan HPS, Lalia BS, Karan K, Maxwell A (2010) Polymer–ionic liquid nano-composites electrolytes: electrical, thermal and morphological properties. Mater Sci Eng B 175:143–149

Morselli D, Bondioli F, Sangermano M, Messori M (2012) Photocured epoxy networks reinforced with TiO_2 in situ generated by means of non-hydrolytic sol-gel process. Polymer 53:283–290

Muir JMR, Idriss H (2013) Computational study of cysteine interaction with the rutile TiO_2 (110) surface. Surf Sci 617:60–67

Muthirulan P, Devi CKN, Sundaram MM (2013) Facile synthesis of novel hierarchical TiO_2@Poly(o-phenylenediamine) core–shell structures with enhanced photocatalytic performance under solar light. J Environ Chem Eng 1:620–627

Okamoto M, John B (2013) Synthetic biopolymer nanocomposites for tissue engineering scaffolds. Prog Polym Sci 38:1487–1503

Pandini S, Baldi F, Paderni K, Messori M, Toselli M, Pilati F, Gianoncelli A, Brisotto M, Bontempi E, Riccò T (2013) One-way and two-way shape memory behaviour of semi-crystalline networks based on sol-gel cross-linked poly(ε-caprolactone). Polymer 54:4253–4265

Park DH, Hwang SJ, Oh JM, Yang JH, Choy JH (2013a) Polymer–inorganic supramolecular nanohybrids for red, white, green, and blue applications. Prog Polym Sci 38:1442–1486

Park SI, Lee EO, Yang HM, Park CW, Kim JD (2013b) Polymer-hybridized liposomes of poly(amino acid) derivatives astrans-epidermal carriers. Colloid Surf B Biointerfaces 110:333–338

Que W, Zhou Y, Chan YC, Kam CH (2000) Optical and microstructural properties of sol-gel derived titania/organically modified silane thin films. Thin Solid Films 358:16–21

Rajesh S, Senthilkumar S, Jayalakshmi A, Nirmala MT, Ismail AF, Mohan D (2013) Preparation and performance evaluation of poly

(amide–imide) and TiO_2 nanoparticles impregnated polysulfone nanofiltration membranes in the removal of humic substances. Colloids Surf A Physicochem Eng Aspects 418:92–104

Sanda F, Endo T (1999) Syntheses and functions of polymers based on amino acids. Macromol Chem Phys 200:2651–2661

Seyedjamali H, Pirisedigh A (2011a) In situ sol–gel fabrication of new poly(amide–ether–imide)/titania (TiO_2) nanocomposite thin films containing L-leucine moieties. Colloid Polym Sci 289:15–20

Seyedjamali H, Pirisedigh A (2011b) Synthesis and morphology of new functional polyimide/titania nano hybrid materials. J Mater Sci 46:6744–6750

Seyedjamali H, Pirisedigh A (2012a) Synthesis of well-dispersed polyimide/TiO_2 nanohybrid films using a pyridine-containing aromatic diamine. Polym Bull 68:299–308

Seyedjamali H, Pirisedigh A (2012b) Well-dispersed polyimide/TiO_2 nanocomposites: in situ sol-gel fabrication and morphological study. Colloid Polym Sci 290:653–659

Singh R, Lillard JW Jr (2009) Nanoparticle-based targeted drug delivery. Exp Mol Pathol 86:215–223

Song G, Zhang Y, Wang D, Chen C, Zhou H, Zhao X, Dang G (2013) Intermolecular interactions of polyimides containing benzimidazole and benzoxazole moieties. Polymer 54:2335–2340

Su C, Shao C, Liu Y (2010) Synthesis of heteroarchitectures of PbS nanostructures well-erected on electrospun TiO_2 nanofibers. J Colloid Interface Sci 346:324–329

Tsai MH, Liu SJ, Chiang PC (2006) Synthesis and characteristics of polyimide/titania nano hybrid films. Thin Solid Films 515:1126–1131

Tsai MH, Chang CJ, Chen PJ, Ko CJ (2008) Preparation and characteristics of poly(amide–imide)/titania nanocomposite thin films. Thin Solid Films 516:5654–5658

Vanherck K, Koeckelberghs G, Vankelecom IFJ (2013) Crosslinking polyimides for membrane applications. Prog Polym Sci 38:874–896

Wu CB, Hao JY, Deng XM (2007) A novel degradable poly(β-amino ester) and its nano-complex with poly(acrylic acid). Polymer 48:6272–6285

Xiao Y, Low BT, Hosseini SS, Chung TS, Paul DR (2009) The strategies of molecular architecture and modification of polyimide-based membranes for CO_2 removal from natural gas. Prog Polym Sci 34:561–580

Xue Y, Tang X, Huang J, Zhang X, Yub J, Zhang Y, Guid S (2011) Anti-tumor efficacy of polymer–platinum(II) complex micelles fabricated from folate conjugated PEG-graft-α, β-poly [(N-amino acidyl)-aspartamide] and cis-dichlorodiammine platinum(II) in tumor-bearing mice. Colloid Surf B Biointerfaces 85:280–281

Yoshida M, Lal M, Kumar ND, Prasad PN (1997) TiO_2 nano-particle-dispersed polyimide composite optical waveguide materials through reverse micelles. J Mater Sci 32:4047–4051